IEEE Photonics Journal
An IEEE Photonics Society Publication

Open Access

Er^{3+}-Doped Nanoengineered Yttria-Stabilized Zirconia Alumino-Silicate Fiber for Efficient CW and Mode-Locked Laser Operation

Volume 8, Number 4, August 2016

Y. W. Lee
J. S. Chang
S. Das
A. Dhar
M. Pal
M. C. Paul
J. T. Lin
Y. W. Jhang

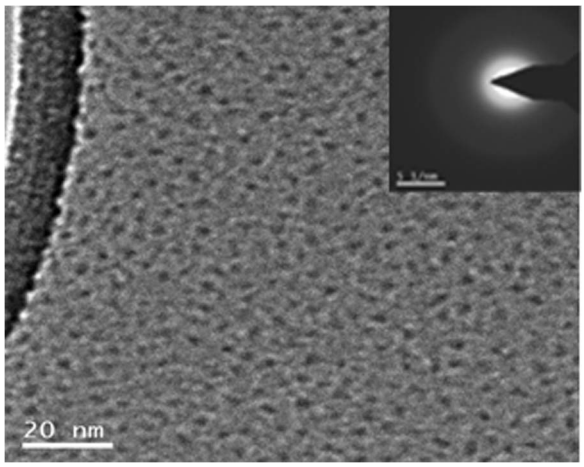

DOI: 10.1109/JPHOT.2016.2585924
1943-0655

IEEE photonics SOCIETY
IEEE

Er^{3+}-Doped Nanoengineered Yttria-Stabilized Zirconia Alumino-Silicate Fiber for Efficient CW and Mode-Locked Laser Operation

Y. W. Lee,[1] J. S. Chang,[1] S. Das,[2] A. Dhar,[2] M. Pal,[2] M. C. Paul,[2] J. T. Lin,[3] and Y. W. Jhang[3]

[1]Department of Electro-optical Engineering, National Taipei University of Technology, Taipei 106, Taiwan
[2]Council of Scientific and Industrial Research-Central Glass and Ceramic Research Institute, Kolkata 196, India
[3]Industrial Technology Research Institute, Tainan 734, Taiwan

DOI: 10.1109/JPHOT.2016.2585924

Manuscript received January 28, 2016; revised June 21, 2016; accepted June 23, 2016. Date of publication June 28, 2016; date of current version July 11, 2016. This work was supported in part by the Ministry of Science and Technology of the Republic of China under Grant 105-2623-E-035-005-D, by the Ministry of Economic Affairs of the Republic of China under Grant 104-EC-17-A-07-S3-011, and by the Royal Society, New Delhi, India. Corresponding authors: Y.-W. Lee and M. C. Paul (e-mail: ywlee@ntut.edu.tw; paulmukul@hotmail.com).

Abstract: We report on the development of efficient continuous wave (CW) and mode-locked ring fiber lasers utilizing an Er^{3+}-doped nanoengineered yttria-stabilized zirconia alumino (YSZA)-silicate fiber as the gain element. With the proper design of the material composition, the YSZA fiber host presents superior features to eliminate the Er^{3+} cluster effects and enhance the radiative emission over commercial silica fibers, thus significantly increasing the fiber laser efficiencies. Through cavity analysis and optimization, we successfully demonstrate a 975-nm pumped single-mode Er^{3+}-doped CW YSZA-silicate fiber laser with a slope efficiency of 43%, which is corresponding to the quantum efficiency of 69%. Because of the special dispersion property of the Er^{3+}-doped YSZA-silicate fiber, we are able to build a stable soliton mode-locked 1565-nm fiber laser with 3.2-nJ pulse energy, 644-fs pulsewidth, and 4.96-kW peak power.

Index Terms: Fiber materials, nanoengineered fiber, zirconia alumino (YSZA)-silicate fiber, Er^{3+}-doped fiber.

1. Introduction

Fiber laser sources in the 1.55-μm eye-safe region are of interest for many applications, such as environmental sensing, eye-safe light detection and ranging (LIDAR), and medical surgery. In recent years, the output power from continuous-wave (CW) and pulsed Er^{3+}-doped fiber lasers and amplifiers has been scaled to the hundred watt and kilowatt level, respectively [1]. However, compared with its counterpart of Yb^{3+} and Tm^{3+} doped fibers, the reported optical efficiency of the Er^{3+}-doped fiber laser is relatively low. This low efficiency mainly comes from upper-state conversion and concentration quenching [2]–[4]. Further power scaling of these fiber laser sources will require higher optical efficiency to avoid detrimental thermal effects. In this connection,

special co-dopants, such as alumina and phosphorus, as well as new host materials such as tellurite and bismuth, have been intensively studied [5]–[8]. Although the concentration quenching phenomenon and cluster formation have been successfully reduced in tellurite [9] and bismuth [10] based fibers, these fibers tend to have low compatibility with passive silica fibers, leading to the difficulty of building all-fiber laser systems. A good alternative approach is to use nano-engineered Er^{3+}-doped zirconia-yttria-alumino (ZYA) silicate glass as the fiber host. The nano-engineered glass with ZrO_2 provides outstanding chemical and physical properties, such as superior hardness, photochemical stability, high optical transparency and thermomechanical resistance [11], [12]. The introduction of Zr^{4+} into an Er^{3+}-doped silicate fiber avoids the cluster formation of Er^{3+} ions and consequently improves the luminescence [13]. In 2013, we demonstrated a simple, compact and low cost graphene based mode-locked nano-engineered Er^{3+}-doped ZYA silicate fiber laser [14]. 400-fs 1561-nm soliton pulses with an 8.5-nm optical bandwidth and 49.5-MHz repetition rate have been successfully generated. Detailed descriptions of the fiber fabrication as well as the optical characteristics of this kind of nano-engineering Er^{3+} doped fiber have already been reported in our earlier work [15]–[19].

As a step further to enhance the optical efficiency for 1.55-μm fiber laser applications, we investigate nano-engineered yttria-stabilized zirconia alumino (YSZA) silicate fiber with more ZrO_2 concentrations. As ZrO_2 has a stretching vibration at about 470 cm^{-1}, which is much lower than that of Al_2O_3 (870 cm^{-1}) and SiO_2 (1100 cm^{-1}) [20], the Er_2O_3 doped phase-separated nanoparticles with a high ZrO_2 concentration possess low phonon energy, which gives rise to increase in the emission cross section, and thus enhances the radiative transition probability between $^4I_{13/2}$ and $^4I_{15/2}$ levels of Er^{3+}. The heavily doped Zr^{4+} ions surround the Er^{3+} ions to form a solvent shell, thereby adjusting the charge balance and improving the solubility of Er^{3+} ions to the host. This inhibits clustering of the Er^{3+} ions and further eliminates concentration quenching. In such an YSZA silicate glass, the ionic refractivity of non-bridging oxygens is larger than that of bridging oxygens [21]. In addition, the large amount of Zr^{4+} ions could change the symmetry of the electron cloud surrounding oxygens. When the intermediate Al_2O_3 in the glass is replaced by the modifier ZrO_2, the number of non-bridging oxygens increases. It is worth noting that the Al^{3+} and Zr^{4+} also act as network modifiers to make the silica network structure more open, although the Al^{3+} ion partially acts as the network former. The open structure is favorable to disperse the Er^{3+} ion in the YSZA silicate glass structure, and thus reduces the clustering phenomenon of Er^{3+} ions. In addition, adding a minute amount of Y_2O_3 can slow down or stop the changes in the ZrO_2 crystalline structure, thereby preserving the mechanical strength and integrity of the fiber. Finally, the employed nano-particle doping process allows us to prohibit the Er^{3+}clustering phenomenon at high doping levels, and enables efficient CW and mode-locked 1.55 μm fiber laser operation. It should be noted that in comparison with germanate and tellurite glass, the main glass network of the silicate fiber is SiO_2, which has strong mechanical strength and better compatibility with conventional passive silica fibers.

We report in this paper our latest progress in the fabrication and material studies of ~900 ppm Er^{3+} doped YSZA silicate fibers. An efficient core-pumped ring-cavity CW fiber laser and stable soliton mode-locked YSZA fiber laser are experimentally demonstrated to prove the good optical efficiency of the Er^{3+}-doped YSZA silicate fiber. The theoretical analysis of the efficient Er^{3+}-doped CW and soliton mode-locked (ML) fiber lasers is also provided.

2. Fiber Fabrication

As shown in Fig. 1, the Er^{3+}-doped YSZA silicate glass fiber preform was made using the modified chemical vapor deposition (MCVD) process, followed by the solution doping technique [16], [17]. The SiO_2 and P_2O_5 glass formers were incorporated through the MCVD process. Al_2O_3, ZrO_2, Er_2O_3, and Y_2O_3 were added as the glass modifiers through the solution doping technique. Incorporation of Y_2O_3 into the host matrix serves the additional purpose of slowing down

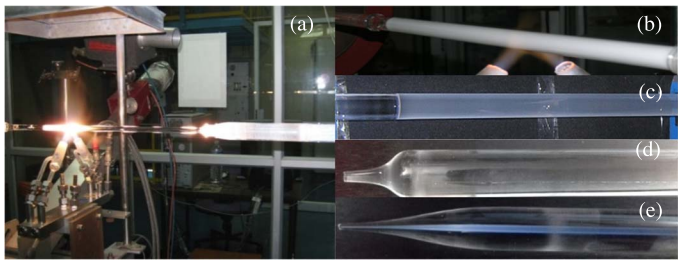

Fig. 1. Fabrication process of Er^{3+}-doped YSZA-silicate glass fiber preform. (a) MCVD process for making the preform at the collapsing stage. (b) Porous phospho-silica soot layer. (c) Solution soaked layer. (d) Optical preform. (e) Annealed preform.

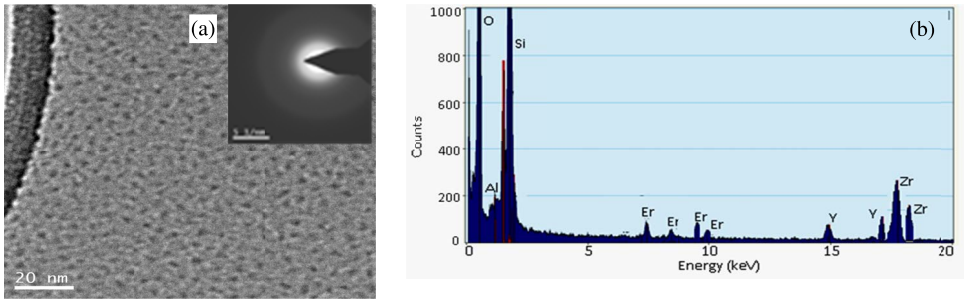

Fig. 2. (a) TEM image of the fiber that was drawn from the annealed preform. (Inset) Electron diffraction pattern. (b) EDX spectra of the phase-separated particles.

or eliminating changes in the ZrO_2 crystal structure [18]. A small amount of P_2O_5 doping was also added in the core matrix of the optical fiber preform and served as a nucleating agent to increase the phase separating phenomenon with the generation of Er_2O_3 doped micro crystallites [19], [20].

To make the nano-engineered Er_2O_3-doped ZrO_2 rich glass fiber, the fabricated preform was annealed at 1100° C for 3 hours with the heating and cooling rates of 20° C/min. The annealed preform shown in Fig. 1(e) is then made to undergo the fiber drawing process, which is the final process of forming the nano-engineered glass based optical fiber. Slight milky whiteness in the core glass appears because of the phase separation phenomenon.

3. Material Properties of Er^{3+}-Doped YSZA Silicate Fibers

By dispersing the fiber in acetone liquid, the morphology of the fiber core glass was studied by transmission electron microscopy (TEM) [Tecnai G^2 30ST, FEI Co]. The nature and composition of nano-particles were evaluated by the electron diffraction and energy dispersive X-ray (EDX) analyses. The nano-phase separated host was retained into the silica glass matrix at the fiber drawing stage as confirmed from TEM analyses along with EDX spectra and electron diffraction patterns, as shown in Fig. 2. The average particle size is around 5 ± 2 nm, and the bright spots in the TEM image illustrate the phase-separated region. The nature of the phase-separated particles was found to be non-crystalline, confirmed by their electron diffraction pattern, as shown in the inset of Fig. 2(a). Diffuse scattering in the electron diffraction reveals the amorphous nature of the particles (see "halo pattern") because of the absence of diffraction spot. The EDX spectrum, as shown in Fig. 2(b), indicates that zirconium, yttrium and erbium are dominant in the phase-separated particles whilst they are found to be negligible in the non-phase-separated areas. In addition, the intensity related to the Al, Zr, Y, and Er ions in the phase-separated particles is much higher than that in the non-phase-separated region. Thus, we can conclude that the majority of the erbium is located in the phase-separated zirconia-yttria-alumina rich region.

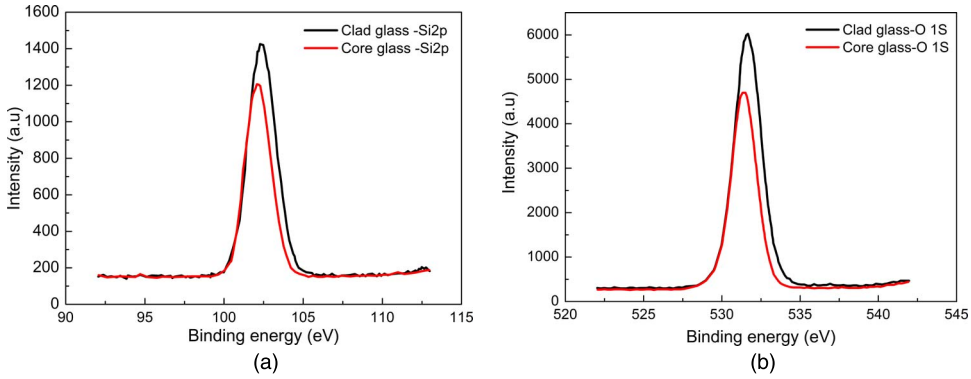

Fig. 3. XPS spectra of (a) Si 2p and (b) O 1 s of the annealed Er^{3+}-doped YSZA fiber preform.

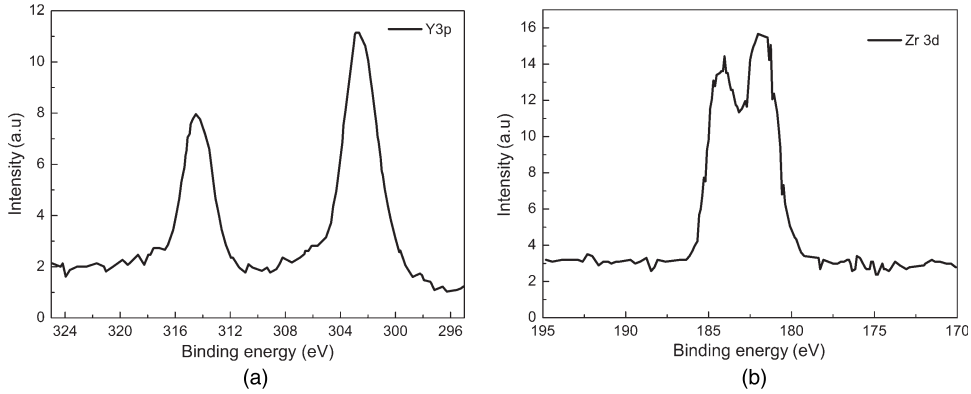

Fig. 4. XPS spectra of (a) Y 3p and (b) Zr 3d for annealed Er^{3+}-doped YSZA fiber preform.

X-ray photoelectron spectroscopy (XPS) was utilized to determine the bond status of erbium in the YSZA optical preform. The characterization of X-ray photo electronic spectroscopy (XPS) was done by introducing the samples into a UHV chamber, equipped with a helium (He) discharge lamp for ultraviolet photoelectron spectroscopy and MgK_{α} X-ray source for XPS. As shown in Fig. 3(a), the binding energy of Si 2p in the core glass is lower than that of the cladding class or silica gel [21]. Such a result indicates the formation of more ionic networks in YSZA glass. Similarly, as shown in Fig. 3(b), the core glass has lower binding energy of oxygen O 1 s than that of the pure silica cladding glass, which confirms more ionic bonding of O and Si.

Fig. 4 indicates the measured XPS spectra of Y 3p and Zr 3d for annealed Er^{3+} doped YSZA fiber preform. The positions of the spin orbit splitting peaks for Y $3p_{1/2}$ and Y $3p_{3/2}$ signals, as shown in Fig. 4(a), are at 314.4 eV and 302.52 eV, respectively. Both values are higher than that of pure silica glass, Y $3p_{1/2}$ (310.6 eV) and Y $3p_{3/2}$ (298.8 eV) [22], because of the presence of electron density deficiency around Y ions. Such decrease in effective electron charge density around the Y ions signifies the increase of the oxygen anions and increases the solubility of Er^{3+} ions. In addition, we observed the binding energy of Zr $3d_{5/2}$ and Zr $3d_{3/2}$ at 182.0 and 184.4 eV, respectively, which suggests the presence of cubic ZrO_2 nanocrystal [23], [24].

4. Geometrical and Spectroscopic Characterization

The mole percentages of various dopants in the fiber were measured by an electron probe micro analyzer (EPMA). As shown in Fig. 5(a), all dopants are distributed uniformly in the core region. Fig. 5(b) is the refractive profile (RI) of the fiber preform, measured by a preform analyzer

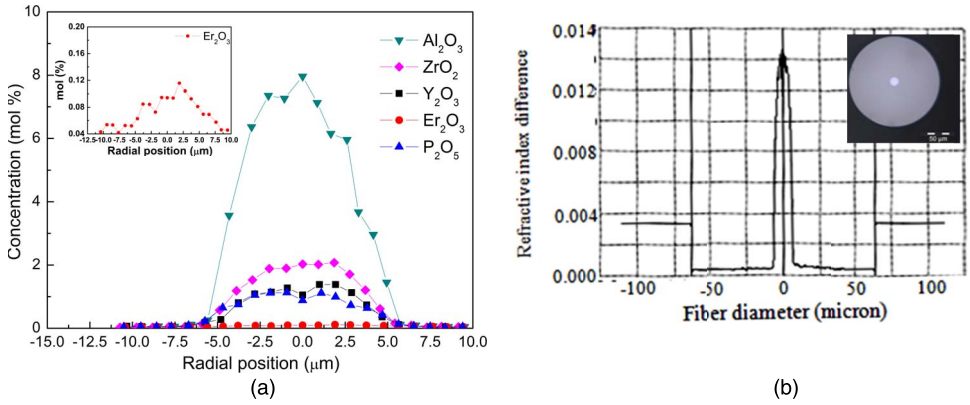

Fig. 5. (a) Distribution curves of the dopants in the core region of YSZA-EDF. (Inset) Er_2O_3 distribution. (b) Fiber refractive index profile. (Inset) Photograph of the fiber.

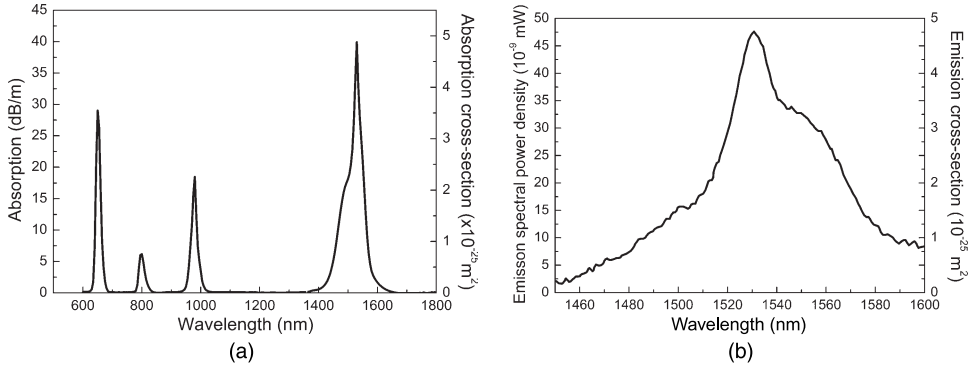

Fig. 6. (a) Absorption and (b) emission spectra and the corresponding cross sections of YSZA-EDF.

(M/s. Photon Kinetics PKI-2600). The sharpness of the RI profile at the core and cladding boundary indicates that the doping elements are distributed uniformly throughout the whole core region of the fiber, which is also confirmed by the EPMA data analysis of the fiber. The microscopic view of the fiber cross-section is shown in Fig. 5(b), measured by an Olympus microscope (model No: BX51).

In general, the glass host composition affects the solubility of the rare-earth dopant and may affect the absorption and emission cross-sections of the dopant transitions. Fig. 6 shows the absorption and emission spectra of the Er^{3+} doped YSZA silicate glass. The absorption curve was obtained using a white-light source through a Bentham spectral attenuation set-up with a fiber output and optical spectrum analyzer (OSA). The spectral shape and absolute scaling of the emission cross-section were determined by applying the McCumber method to the measured peak absorption cross-section [25]. The results indicate that the spectra of Er^{3+} ions in YSZA silicate glass are fairly similar to that in commercial silica glass. Although the McCumber method has been shown to be rather inaccurate in rare-earth doped glass fibers when precise cross-section values are required [26], it provides a convenient estimate for the related theoretical modeling in this work.

The decay of the intensity of the luminescence ($^4I_{13/2}$ to $^4I_{15/2}$ of the Er^{3+} energy levels) was also carefully measured with a 976-nm core-pumped cm-long fiber sample. The fiber sample was angle-cleaved to prevent any feedback. The pump laser diode was modulated to achieve square-shaped pulses of ms-width with sharp rise and fall edges under a time resolution of 8 μs. The measured data were fitted to an exponential curve to determine the effective lifetime. As shown in Fig. 7, the upper state lifetime was found to be around 10.47 ± 0.015 ms. In addition,

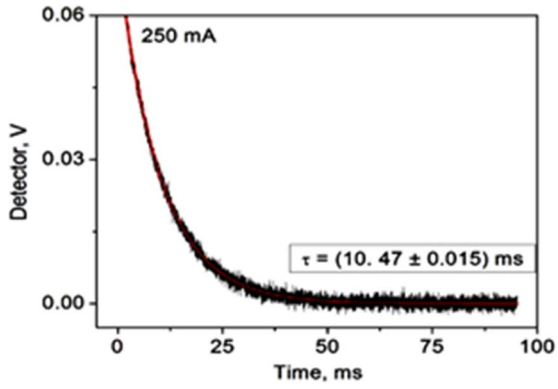

Fig. 7. Measured fluorescence decay curve of Er^{3+}-doped YSZA fiber.

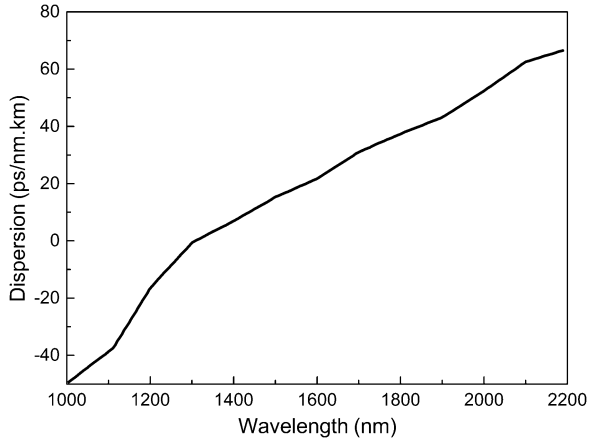

Fig. 8. Chromatic dispersion curve of the Er^{3+}-doped YSZA fiber.

the measured fluorescence relaxation curve showed a single exponential, thus demonstrating negligible concentration quenching.

Fig. 8 shows the dispersion of the Er^{3+} doped YSZA fiber, measured with a Mach–Zehnder interferometer. The zero dispersion is located at 1290 nm. The background loss of the fiber was also checked using a high-resolution optical time-domain reflectometer (OTDR, Luciol). The background loss at 1285 nm was found to be between 50–110 dB/km.

5. Demonstration of Efficient CW Ring Fiber Laser

The experimental setup for the CW Er^{3+}-doped ring fiber laser is shown in Fig. 9. The employed Er^{3+}-doped YSZA silicate fiber has a 10-μm core diameter with NA of 0.149. Good mode transformation between such a slightly multi-mode gain fiber to single mode passive fiber, SMF28, was achieved through active fiber splicing with proper splice duration and current. The output beam was in the fundamental fiber mode (LP_{01}) and was of excellent quality, as expected for a single-mode SMF28 fiber ring cavity. The 2-m fiber length was chosen to get more than 20 dB pump absorption at 974.6 nm, verified through both theoretical simulation and experimental measurement. A directional coupler served as the output coupler of the ring cavity. Without the use of wavelength filtering devices, the laser wavelength was naturally selected through the gain competition. The residual pump power was filtered by another WDM, and the signal was then sent to either a power meter or an optical spectrum analyzer.

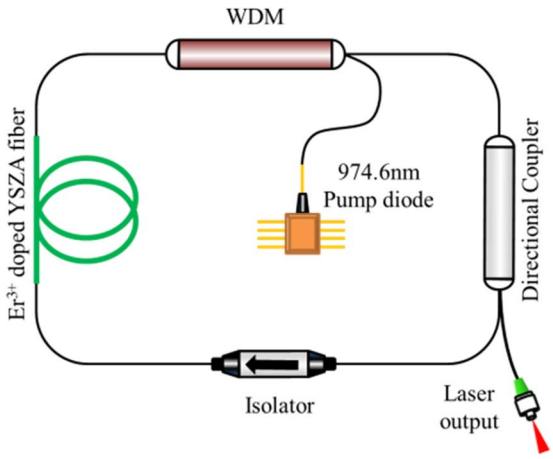

Fig. 9. Experimental setup of the Er^{3+}-doped YSZA ring fiber laser.

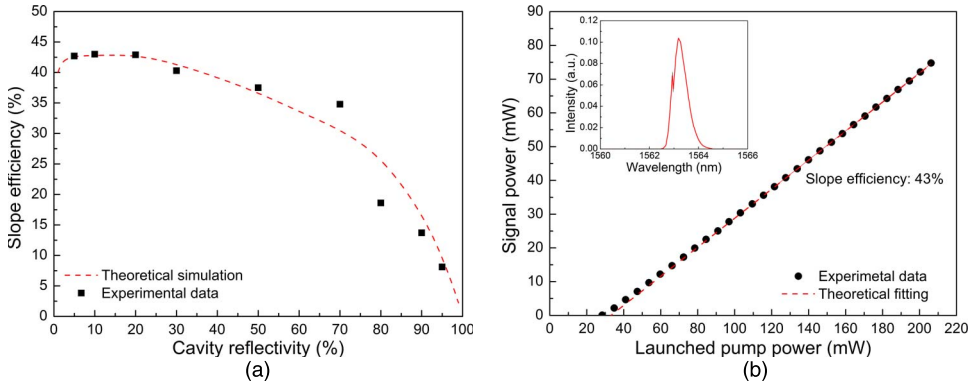

Fig. 10. (a) Laser slope efficiency as a function of cavity reflectivity in the Er^{3+}-doped YSZA-silicate ring fiber laser. (b) Measured output power of the laser with 5% reflectivity as a function of the pump power (dots) and linear fit to the data (solid curve). (Inset) Laser output spectrum under the 200-mW pump power.

Choosing a proper cavity reflectivity is essential to manipulate laser wavelength and optimize the laser efficiency. To correctly evaluate the Er^{3+}-doped YSZA silicate fiber laser with various cavity reflectivities, LIEKKI™ Application Designer v4.0 was employed for the numerical modeling [27]. This code solves the coupled laser rate equations numerically to predict the output performance of the fiber laser sources. The abovementioned absorption and emission cross-sections, propagation loss, and upper state lifetime were employed in the following theoretical simulation.

The measured and the theoretically simulated laser slope efficiency as a function of the cavity reflectivity curve are shown in Fig. 10(a). The experimental data are in good agreement with the simulation results. Both results indicate that the lower cavity reflectivity is, the higher laser slope efficiency can be achieved. In addition, the output power was not very sensitive in the low reflectivity region. The highest slope efficiency of 43% is reached under the 10% cavity reflectivity. The output power versus pump power of the fiber laser with 10% reflectivity is presented in Fig. 10(b). With the 975-nm pumping, the corresponding quantum efficiency is as high as 69%. In general, a core-pumped Er^{3+}-doped fiber laser exhibits high population inversion and its slope efficiency could be easily degraded because of Er^{3+} clustering. Although the 59% slope efficiency has been achieved in a 980-nm core-pumped Er^{3+}-doped fiber amplifier [28], the relatively low Er^{3+} ion concentration (~100 ppm) is required to obtain such a high efficiency. The

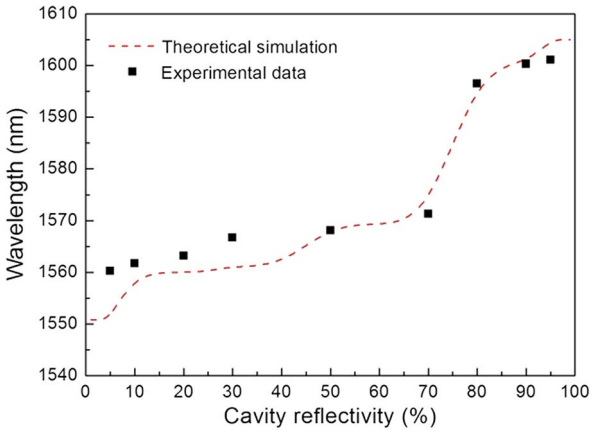

Fig. 11. Measured (dot) and simulated (dash curve) laser output spectrum as a function of cavity reflectivity.

measured 43% slope efficiency in this work successfully verifies the good optical property of the employed ~900-ppm Er^{3+}-doped YSZA silicate fiber. The output spectrum of the fiber laser with its peak at 1563.2 nm is shown in the inset of Fig. 10(b).

Fig. 11 represents the experimental results and theoretical prediction of the laser wavelength as a function cavity reflectivity with a fixed gain fiber length of 2 m. The FWHM linewidths of all lasers are narrower than 1 nm. The results indicate that the lasers with relatively high reflectivities lase at relatively long wavelengths, which can be expected based on the gain competition [29]. In general, for the cavities with low reflectivity, the circulated signal power in the gain fiber is relatively small, and thus the short wavelengths with higher absorption and emission cross-sections tend to accumulate energy and emit lasers. Nevertheless, for the cases with high reflectivity, the gain at short wavelengths is first saturated because of the large circulated signal power, and thus the laser emission is established at long wavelengths. The longest wavelength of 1601 nm can be easily achieved under the 95% cavity reflectivity.

6. Demonstration of Efficient Soliton Mode-Locked Ring Fiber Lasers

The schematic of the mode-locked Er^{3+}-doped silicate ring fiber laser is shown in Fig. 12. The setup is similar to the one shown in Fig. 3, except that the additional devices include an in-line polarizer (ILP) and two polarization controllers (PCs) to enable nonlinear polarization evolution (NPE) mode-locking operation [30]. An autocorrelator, optical spectrum analyzer, oscilloscope and radio-frequency (RF) spectrum analyzer along with a 2 GHz photo detector were used to simultaneously monitor the output pulse shape, laser spectra and pulse train or RF spectrum, respectively.

The passively CW mode-locked laser pulses were generated through proper adjustment of two PCs under the launched pump power of more than 83 mW. Fig. 13 illustrates the measured output power and calculated pulse energy as a function of pump power under four cavity reflectivities. The highest slope efficiency of 22.6% was reached under the 5% cavity reflectivity. At the pump power of 215 mW, the signal output power reached its maximum output power of 36 mW with the corresponding pulse energy of 3.2 nJ. When the pump power was further increased, the single mode-locking pulses started to split into two or three pulses because of the upper limit of the soliton fiber laser pulse energy. This limit is determined by laser parameters, including saturable absorber's saturation energy, modulation depth, cavity dispersion, and self-phase-modulation [31]. Such multiple mode-locking reduced the pulse energy and stability. It is worth noting that the ML laser with 30% reflectivity shows the energy rollover and pulse instability with the relatively lower pump power. This is because the relatively high cavity Finesse leads to large circulated signal peak powers and generates nonlinear processes inside the cavity.

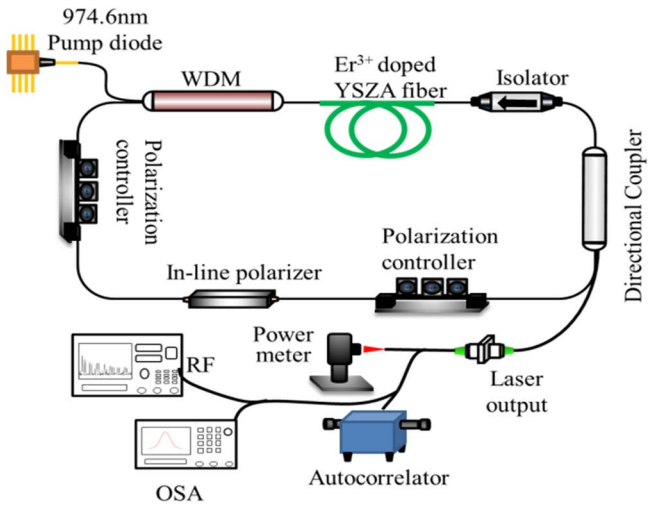

Fig. 12. Schematic of the mode-locked Er^{3+}-doped YSZA-silicate ring fiber laser.

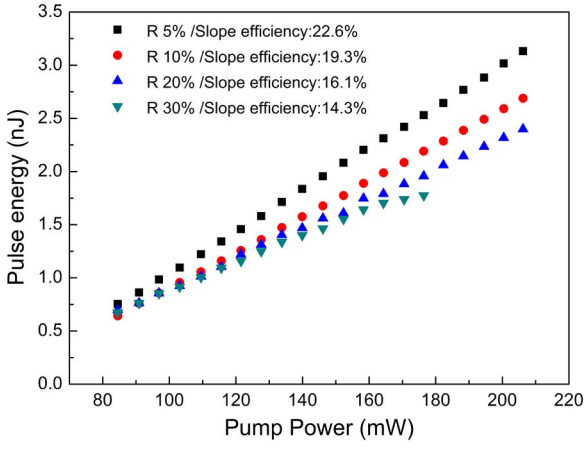

Fig. 13. Output power as a function of the pump power of the mode-locked Er^{3+}-doped YSZA-silicate ring fiber laser under different cavity reflectivities.

The oscilloscope trace and RF spectrum of the CW-ML laser with a cavity reflectivity of 5% are shown in Fig. 14(a) and (b). Both results indicate that the repetition rate of the uniform pulse train is 11.2 MHz. The relatively long cavity is owing to the long passive fibers used in the mechanical PCs. The inset figure of Fig. 14(b) shows the wideband RF spectrum up to 300 MHz. The absence of spectral modulation in the RF spectrum indicates that the laser operates well in the CW mode-locking regime.

The autocorrelation traces of the aforementioned fiber laser with 5% cavity reflectivity under four pump powers are also presented in Fig. 15(a). All of the generated laser pulses have the squared hyperbolic secant ($sech^2$) profile. Fig. 15(b) shows one example, measured under the pump power of 206 mW. The output pulse has a measured FWHM of 993.69 fs, which corresponds to a 644-fs $sech^2$ pulse width through the deconvolution factor 1.543 [32]. The derived $sech^2$ pulse widths for each pump power are also shown in Fig. 15(a). The results indicate that the pulse width decreases with the increase of the pump power. The calculated peak power of the 3.2 nJ pulse is as high as 4.96 kW, which successfully verifies the good optical property and strong mechanical strength of the Er^{3+}-doped YSZA fiber.

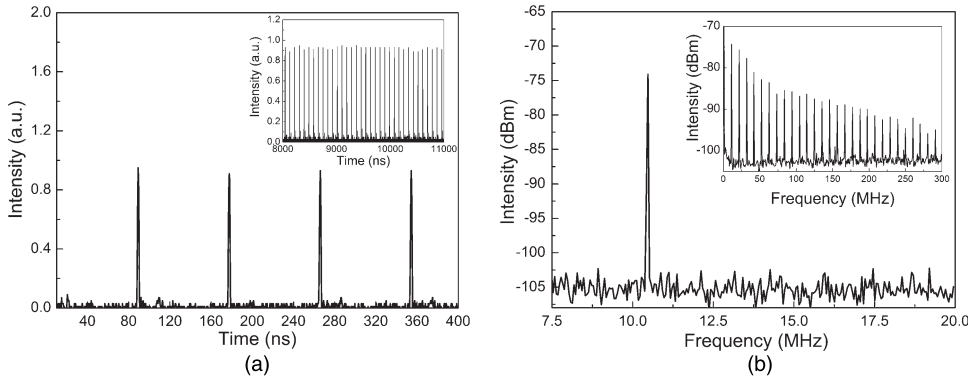

Fig. 14. (a) Time trace. (b) RF spectrum of the mode-locked fiber laser with 5% cavity reflectivity.

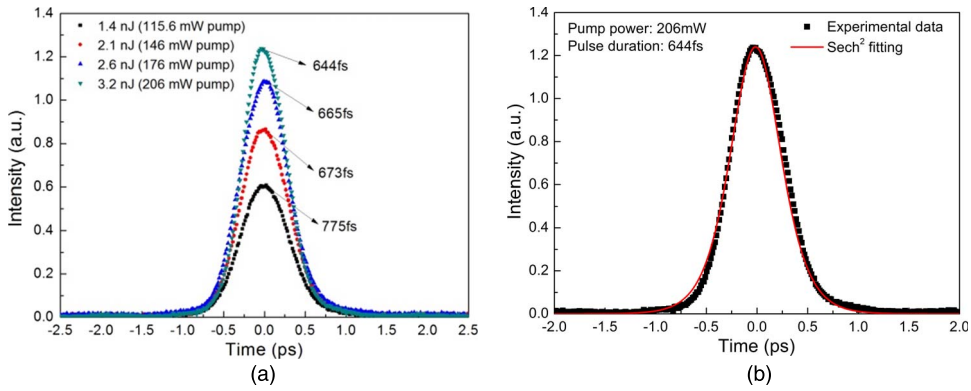

Fig. 15. (a) Measured autocorrelation trace of the mode-locked Er^{3+}-doped YSZA-silicate ring fiber laser under different pump powers. (b) (Dark dot) Measured and (red line) hyperbolic-secant-fitted autocorrelator curves.

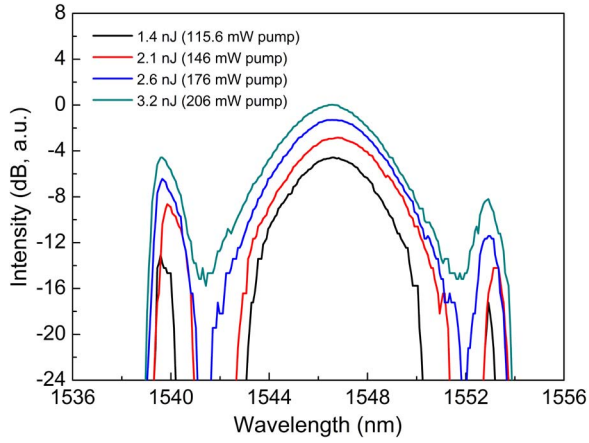

Fig. 16. Measured output spectrum of the mode-locked fiber laser with 5% reflectivity as a function of the pump power.

The laser output spectrum as a function of pump power is illustrated in Fig. 16. All of these spectra have a broad spectral bandwidth centered at 1546.5 nm. The 3 dB bandwidth of the 3.2 nJ pulse is about 4.0 nm, corresponding to a time-bandwidth product (TBP) of 0.322. The

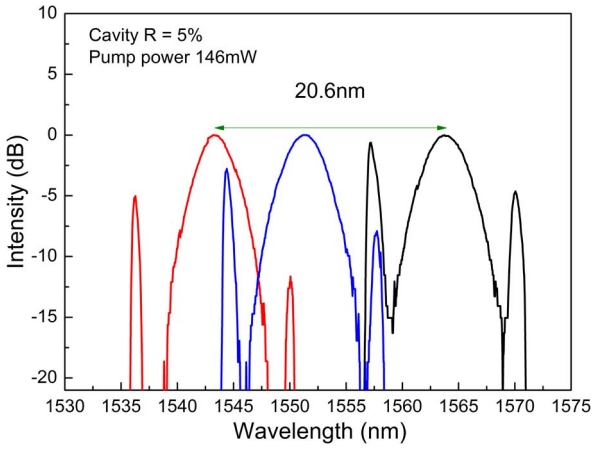

Fig. 17. Wavelength-tuned Er^{3+}-doped YSZA-silicate mode-locked fiber laser.

net cavity dispersion of the employed ring fiber laser cavity is estimated as -0.395 ps^2. Such negative net cavity dispersion is also verified by the exhibition of Kelly sidebands [33]. In addition, by measuring the wavelength separation between the 1st order sideband and center wavelength $(\Delta\lambda)$, the net cavity dispersion under the laser operation can be derived based on (see [34])

$$\beta_2 L = \frac{-\lambda_0^2}{\pi c^2}\left[\left(\frac{\Delta\lambda}{\lambda_0}\right)^2 + \frac{\ln^2(1+\sqrt{2})}{\pi^2}\left(\frac{\lambda_0}{c\Delta\tau}\right)^2\right]^{-1} \tag{1}$$

where $\Delta\tau$ is the pulse temporal FWHM, λ_0 is the center wavelength, and c is the speed of light. For the case with pulse energy of 3.2 nJ, $\Delta\tau$ of 644 f_s and $\Delta\lambda$ of 6.4 nm, the corresponding net cavity dispersion under the laser operation is -0.385 ps^2. The derived cavity dispersion is slightly larger yet close to the calculated net cavity dispersion of -0.395 ps^2. The result indicates that the self-phase- modulation contributes a certain amount of positive dispersion because of the high peak power.

The laser wavelength can be further tuned by adjusting two intra-cavity PCs during the mode locking operation. The laser output spectra with different center wavelengths are shown in Fig. 17. The leftmost spectrum is centered at 1543 nm with a FWHM bandwidth of ~3.8 nm and output power of 35 mW, while the rightmost spectrum shows the mode-locked laser at center wavelength 1565 nm without change of the laser output power. The wavelength tuning range can be as large as 20.6 nm.

7. Conclusion

In conclusion, we have investigated the essential material properties of Er^{3+} doped YSZA silicate fiber as well as its potential for applications in efficient CW and mode-locked fiber lasers. Such a fiber gain medium not only has high solubility for Er^{3+} ions, but also has a larger phonon energy resulting in more efficient energy transfer. The presented material studies include the measurement of fiber absorption and emission spectra, upper-state lifetime, chromatic dispersion and background loss. These study results allow us to precisely evaluate the output performance of the 900-ppm Er^{3+}-doped YSZA silicate fiber. In addition, we present the experimental evidence of a ring cavity CW single-mode fiber laser with 43% of the slope efficiency and a stable soliton mode-locked fiber laser with the 3.2-nJ pulse energy and 644-fs pulse width at 1565 nm. To the best of our knowledge, 43% is the best slope efficiency from a CW Er^{3+}-doped zirconia-alumino silicate fiber laser. The corresponding quantum efficiency of 69% indicates no quenching phenomenon is observed in the gain fiber even under the high population

inversion. All of the results indicate that this Er^{3+}-doped YSZA fiber could have significant advantages for generating efficient CW and high-peak power mode-locked 1.56-μm fiber lasers.

References

[1] M. N. Zervas and C. A. Codemard, "High power fiber lasers: A review," *IEEE J. Sel. Top. Quantum Electron.*, vol. 20, no. 5, Sep./Oct. 2014, Art. no. 0904123.

[2] J. L. Wagener, P. F. Wysocki, M. J. F. Digonnet, H. J. Shaw, and D. J. DiGiovanni, "Effects of concentration and clusters in erbium-doped fiber lasers," *Opt. Lett.*, vol. 18, no. 23, pp. 2014–2016, Dec. 1993.

[3] A. V. Kir'yanov, Y. O. Barmenkov, G. E. Sandoval-Romero, and L. Escalante-Zarate, "Er^{3+} concentration effects in commercial Erbium-doped silica fibers fabricated through the MCVD and DND technologies," *IEEE J. Quantum Electron.*, vol. 49, no. 6, pp. 511–520, Jun. 2013.

[4] E. Snoeks, P. G. Kik, and A. Polman, "Concentration quenching in erbium implanted alkali silicate glasses," *Opt. Mater.*, vol. 5, no. 3, pp. 159–167, Mar. 1996.

[5] S. Jiang *et al.,* "Net gain of 15.5 dB from a 5.1 cm-long Er^{3+}-doped phosphate glass fiber," in *Proc. Tech. Dig. Opt. Fiber Commun. Conf., Post deadline*, 2000, pp. 181–183.

[6] Z. Qiang, J. Geng, T. Luo, J. Zhang, and S. Jiang, "High-efficiency ytterbium-free erbium-doped all-glass double cladding silicate glass fiber for resonantly-pumped fiber lasers," *Appl. Opt.*, vol. 53, no. 4, pp. 643–647, Feb. 2014.

[7] Y. Ohishi, A. Mori, M. Yamada, H. Ono, Y. Nishida, and K. Oikawa, "Gain characteristics of tellurite-based erbium-doped fiber amplifiers for 1.5-μm broadband amplification," *Opt. Lett.*, vol. 23, no. 4, pp. 274–276, Feb. 1998.

[8] X. S. Cheng, R. Parvizi, H. Ahmad, and S. W. Harun, "Wide-band bismuth-based erbium-doped fiber amplifier with a flat-gain characteristic," *IEEE Photon. J.*, vol. 1, no. 5, pp. 259–264, Nov. 2009.

[9] Z. Jia, H. Li, X. Meng, L. Liu, G. Qin, and W. Qin, "Broadband amplification and highly efficient lasing in erbium-doped tellurite microstructured fibers," *Opt. Lett.*, vol. 38, no. 7, pp. 1049–1051, Jan. 2013.

[10] S. W. Harun, R. Akbari, H. Arof, and H. Ahmad, "Mode-locked bismuth-based erbium-doped fiber laser with stable and clean femtosecond pulses output," *Laser Phys. Lett.*, vol. 8, no. 6, pp. 449–452, Jan. 2011.

[11] D. E. Harrison, N. T. Melamed, and E. C. Subbarao, "A new family of self-activated phosphors," *J. Electro chem. Soc.*, vol. 110, no. 1, pp. 23–28, Jan. 1963.

[12] C. Urlacher, J. Dumas, J. Serughetti, J. Mugnier, and M. Munoz, "Planar ZrO_2 waveguides prepared by the sol-gel process," *Sol-Gel Sci. Technol.*, vol. 8, no. 1, pp. 999–1005, Nov. 1997.

[13] G. Brasse *et al.,* "Nanoscaled optical fibre obtained by the sol-gel process in the $SiO_2 - ZrO_2$ system doped with rare earth ions," *Opt. Mater.*, vol. 31, no. 5, pp. 765–768, Mar. 2009.

[14] M. C. Paul, G. Sobon, and J. Sotor, "A graphene-based mode-locked nano-engineered zirconia-yttria-alumino-silicate glass based erbium-doped fiber laser," *Laser Phys.*, vol. 23, no. 3, pp. 035110–035116, Feb. 2013.

[15] H. Ahmad, K. Thambiratnam, M. C. Paul, and S. W. Harun, "Single-longitudinal-mode operation in tunable novel zirconia-yttria-alumina-erbium-doped fiber laser," *Laser Phys.* vol. 24, no. 8, pp. 085106–085111, Jul. 2014.

[16] M. C. Paul *et al.,* "Wide band EDFA based on erbium doped crystalline zirconia yttria alumino silicate fiber," *IEEE J. Lightw. Technol.*, vol. 28, no. 20, pp. 2919–2924, Oct. 2010.

[17] M. C. Paul *et al.,* "Performance comparison of Zr-based and Bi-based erbium-doped fiber amplifiers," *Opt. Lett.*, vol. 35, no. 17, pp. 2882–2884, Sep. 2010.

[18] K. Thambiratnam, A. Z. Zulkifli, and M. C. Paul, "Fabrication and application of Zirconia-Erbium doped fibres," *Opt. Mater. Exp.*, vol. 2, no. 12, pp. 1690–1701, Dec. 2012.

[19] K. Thambiratnam *et al., "Q-switching and mode-locking in highly-doped* $ZrO_2 - Al_2O_3 - Er_2O_3$ *doped fiber lasers using graphene as a saturable absorber," IEEE J. Sel. Top. Quantum Electron.*, vol. 20, no. 1, pp. 1100108–1100115, Jan./Feb. 2014.

[20] A. Patra, C. S. Friend, R. Kapoor, and P. N. Prasad, "Upconversion in Er^{3+} : ZrO_2 nanocrystals," *J. Phys. Chem. B.*, vol. 106, no. 8, pp. 1909–1912, Feb. 2002.

[21] W. D. Kingery, H. K. Bowen, and D. R. Uhlmann, *Introduction to Ceramics*, vol. 626. New York, NY, USA: Wiley, Mar. 1976.

[22] V. Simon, D. Eniu, A. Takac, K. Magyari, M. Neumann, and S. Simon, "X-ray photoemission study of yttrium contained in radiotherapy systems," *J. Optoelectron. Adv. Mater.*, vol. 7, no. 6, pp. 2853–2857, Dec. 2005.

[23] K. A. Kawasaki, "Positions of photoelectron and auger lines on the binding energy scale," in *Proc. Japan XPS Int.*, 1997, pp. 1–7.

[24] S. Ram and A. Mondal, "X-ray photoelectron spectroscopic studies of Al^{3+} stabilized ZrO^2 of nanoparticles," *Appl. Sur. Sci.*, vol. 221, no. 1–4, pp. 237–247, Jan. 2004.

[25] D. E. McCumber, "Theory of phonon terminated optical masers," *Phys. Rev. Lett.*, vol. 134, no. 2A, pp. 299–306, Jan. 1964.

[26] M. J. F. Digonnet, E. Murphy-Chutorian, and D. G. Falquier, "Fundamental limitations of the McCumber relation applied to Er-doped silica and other amorphous-host lasers," *IEEE J. Quantum Electron.*, vol. 38, no. 12, pp. 1629–1637, Dec. 2002.

[27] Y. W. Lee, H. W. Chien, C. H. Cho, J. Z. Chen, J. S. Chang, and S. Jiang, "Heavily Tm^{3+}-doped silicate fiber for high-gain fiber amplifiers," *Opt. Mater. Exp.*, vol. 5, no. 13, pp. 549–557, Dec. 2015.

[28] R. I. Laming, J. E. Townsend, D. N. Payne, and F. Meli, "High-power erbium-doped-fiber amplifiers operating in the saturated regime," *IEEE J. Light. Technol.*, vol. 3, no. 3, pp. 253–255, Mar. 1991.

[29] D. Venkitesh and R. Vijaya, "A tunable erbium doped fiber ring laser without the use of intra cavity filters," *Photon. North*, vol. 6796, pp. 6796111–6796118, Jun. 2007.

[30] J. H. Lin *et al.,* "Near-infrared supercontinuum generation in single-mode nonlinear Yb^{3+}-doped fiber amplifier," *Opt. Exp.*, vol. 22, no. 13, pp. 16130–16138, Jun. 2014.
[31] Q. Wang, J. Geng, T. Luo, and S. Jiang, "Mode-locked 2 μm laser with highly thulium-doped silicate fiber," *Opt. Lett.*, vol. 34, no. 23, pp. 3616–3618, Dec. 2009.
[32] Q. Bao *et al.,* "Atomic-layer graphene as a saturable absorber for ultrafast pulsed lasers," *Adv. Function. Mater.*, vol. 19, no. 19, pp. 3077–3083, 2009.
[33] S. M. J. Kelly, "Characteristic sideband instability of periodically amplified average soliton," *Electron. Lett.*, vol. 28, no. 8, pp. 806–808, Jan. 1992.
[34] M. L. Dennis and I. N. Duling, III, "Experimental study of sideband generation in femtosecond fiber laser," *IEEE J. Quantum Electron.*, vol. 30, no. 6, pp. 1469–1477, Jun. 1994.